



Design of aperiodic demultiplexers and optical diodes by optimizing photonic crystals

BOAZ BLANKROT*  AND CLEMENS HEITZINGER

Institute of Analysis and Scientific Computing, TU Wien, Wiedner Hauptstrasse 8–10, 1040 Vienna, Austria

**boaz.blankrot@tuwien.ac.at*

Abstract: We apply a previously developed approach for the automated design of optical structures to two cases. This approach reduces the basis of the electromagnetic system to obtain fast gradient-based optimization. In the first case, an existing photonic crystal demultiplexer is optimized for higher power transmission and lower crosstalk. In the second, new optical diodes for plane- and cylindrical-wave incidence are designed using a photonic crystal as a starting point. Highly efficient and aperiodic devices are obtained in all cases. These results indicate that aperiodic devices produced by this automated design method can outperform their analytically-obtained counterparts and encourage its application to other photonic crystal-based devices.

Published by The Optical Society under the terms of the [Creative Commons Attribution 4.0 License](https://creativecommons.org/licenses/by/4.0/). Further distribution of this work must maintain attribution to the author(s) and the published article's title, journal citation, and DOI.

1. Introduction

Photonic crystals, metamaterials, and other optical nanostructures have been attracting interest due to their unique and effective light-manipulation abilities. The advent of optical computing has brought the promise of higher bandwidth and lower energy dissipation [1], at the cost of reinventing traditional electrical structures for photonics, such as diodes, logical gates [2,3], and demultiplexers. Demultiplexers are crucial for splitting optical signals in photonic circuits in general, but particularly for the goal of all-optical computing, and have been designed via e.g. arrayed-waveguide gratings [4], microring resonators [5], shape optimization [6], and photonic crystals [7–9]. Passive optical diodes, or devices that allow asymmetrical optical transmission, have been of great interest due to their potential as building blocks in optical computing and communication. As such, they have been developed using a variety of methods, including nonlinearity [10], magneto-optical effects [11], metamaterials [12,13], gratings [14,15], and photonic crystal-based structures [16–18]. Photonic crystals for these applications are typically periodic with the exception of defects introduced to the design for specific light localization properties. However, in [19], the advantage of exploring aperiodic layouts was demonstrated by showing via statistical analysis that their additional degrees of freedom allow better control of the electromagnetic fields. As expected, this phenomenon was more pronounced in the near field, which is the region of interest in photonic crystal design. Previous results in [20] suggest that better focusing of light can be achieved via optimization which yields irregular layouts. The restrictive nature of periodic structures is also apparent when designing multi-frequency photonic crystal devices using bandgap information; often, the range of compatible frequencies is somewhat restricted by the geometry.

In this work, we present aperiodic two-dimensional nanostructures consisting of circular silicon rods in air which were automatically designed for two applications: multiplexing and one-way transmission of transverse magnetic (TM) waves. The work herein builds upon an optimization approach for the design of photonic structures introduced in [20] and later extended to multiple-frequency devices such as demultiplexers in [21]. In this approach, rods are replaced with multipole expansions and the interactions between them are described as a compressed

multiple-scattering system [22,23]. This system is analytically differentiable as a function of the rod radii, facilitating fast gradient-based optimization. We believe these devices are not only useful for the applications outlined above, but also that the methodology used to design them may be applied to better many other photonic structures.

Prior work on optimizing photonic structures has used e.g. topology optimization [24], with finite differences or finite elements as the underlying electromagnetic solver, which requires computationally expensive and repetitive solutions with many degrees of freedom. Conversely, our method represents each rod with a small multipole expansion, substantially compressing the electromagnetic system of equations. In [25], genetic optimization of a small number of parameters in photonic crystal slab cavities obtained optimal quality factors, though the wave expansion required a large basis which inevitably led to long run times. Recently, a periodic photonic-crystal-based LED structure was optimized for color conversion in [26] where a homogenization technique was applied to the unit cell. In contrast, our approach allows for aperiodic solutions, whether in radii or in location.

2. Formulation of our approach

We assume an arbitrary layout of M dielectric circular rods with radii R_m in two-dimensional space. Our goal is to optimize a function $f(P_i(\ell_j))$ where i denotes a specific combination of wavelength, refractive index, and incident field, and ℓ_j is a curve through which power flow is calculated, such that

$$P_i(\ell_j) = \frac{1}{2} \Re \int_{\ell_j} (\mathbf{E}_i \times \mathbf{H}_i^*) \cdot \hat{\mathbf{n}} \, dl. \quad (1)$$

For each setting $i = 1, \dots, I$, we use the multiple-scattering formulation to arrive at our system of equations

$$(\mathbf{I} - \mathbf{X}_i \mathbf{T}_i) \boldsymbol{\beta}_i = \mathbf{X}_i \boldsymbol{\alpha}_i, \quad (2)$$

where \mathbf{X}_i is a diagonal scattering matrix that additionally depends on the radius of the rods, and \mathbf{T}_i is a translation matrix that depends on the distances between the rods. $\boldsymbol{\alpha}_i$ are the resulting coefficients of expanding the incident field with Bessel functions, $\boldsymbol{\beta}_i$ are the outgoing multipole coefficients, and the residuals of these systems are denoted by \mathbf{c}_i . As the multipole expansion yields the representation $E_{i,z}(\mathbf{r}) = \mathbf{e}_{i,z}(\mathbf{r}) \cdot \boldsymbol{\beta}$, and similar representations for $H_{i,x}$, $H_{i,y}$, we can find the derivatives of the power with respect to these coefficients, $\partial P_i / \partial \boldsymbol{\beta}_i$. We can now construct the gradient of f with respect to the radii for our optimization problem using the adjoint method [27]. For complex vectors $\boldsymbol{\zeta}_i$, we define the Lagrangian

$$\Lambda = f + 2 \Re \sum_i \boldsymbol{\zeta}_i^\top \mathbf{c}_i, \quad (3)$$

whose total derivative with respect to one of the radii R_m can be written as follows using the chain rule,

$$\frac{d\Lambda}{dR_m} = 2 \Re \sum_i \left(\boldsymbol{\zeta}_i^\top (\mathbf{I} - \mathbf{X}_i \mathbf{T}_i) + \frac{\partial f}{\partial \boldsymbol{\beta}_i} \right) \frac{\partial \boldsymbol{\beta}_i}{\partial R_m} - \boldsymbol{\zeta}_i^\top \frac{\partial \mathbf{X}_i}{\partial R_m} \mathbf{X}_i^{-1} \boldsymbol{\beta}_i. \quad (4)$$

Equating the expression in the parentheses with zero and solving the resulting adjoint systems of equations for $\boldsymbol{\zeta}_i$, which does not depend on m , means that the right-hand side of Eq. (4) can be computed for all values of m with I system solutions. On the other hand, since we are solving for $\mathbf{c}_i = 0$, we know that the total derivatives of Λ and f are equal. Finally, the derivatives of the scattering matrices are computed analytically as a combination of Bessel and Hankel functions. Thus both f and its gradient can be computed with the runtime complexity of $2I$ system solutions, which in our case are accelerated with the Fast Multipole Method [28].

3. Results and discussion

We first consider a two-input demultiplexer, or diplexer, where we take as a reference design the device conceived in [29]. The device consists of a T-junction with a line defect input waveguide where the bulk photonic crystal has rod radius $r/a = 0.18$ and a bandgap for $\omega a/2\pi c = 0.303 - 0.444$, for unit cell size a . In that work, both the selection of operating frequencies and the design of the output waveguides were tuned manually such that the two dispersion curves exhibited specific characteristics. This reference design was chosen since it was highly efficient to begin with, and therefore any improvements achieved using optimization would lend support to our method. This reference design is depicted in Fig. 1, where the unit cell size is $a = 1 \mu\text{m}$, the refractive index of the rods is $n = 3.4$, and the two normalized input frequencies are $a/\lambda_1 = 0.387$, $a/\lambda_2 = 0.336$. The diplexer is excited by a current filament, and the desired outputs for λ_1 , λ_2 are on the left and right sides, respectively.

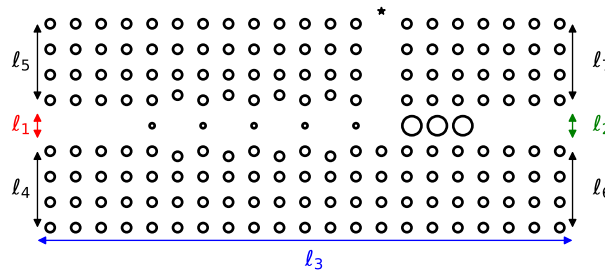


Fig. 1. Diplexer before optimization. Unit cell size is $a = 1 \mu\text{m}$, lines indicate arcs through which the propagated power was calculated for optimization. Black star denotes the input current filament location.

We simultaneously optimized the radii of the 172 rods in this design to maximize desired power flow while minimizing crosstalk and leakage by minimizing the objective function

$$f = \sum_{i=1,2} \frac{P_{3-i}(\ell_i)}{P_i(\ell_i)} + \frac{P_i(\ell_3)}{P_i(\ell_i)} + \frac{P_i(\ell_{2i+2})}{P_i(\ell_i)} + \frac{P_i(\ell_{2i+3})}{P_i(\ell_i)} + C \max(0, 1 - \frac{P_i(\ell_i)}{P_i^*})^2, \quad (5)$$

where $P_i(\ell_j)$ is the power flow of the i -th wavelength propagating through the arc ℓ_j ; the arcs are shown in Fig. 1. For each value of i , the first summand minimizes crosstalk, the last summand penalizes solutions where the output power is smaller than a predetermined quantity, and the other summands represent power leakage through the bottom and sides of the bulk photonic crystal. P_1^* , P_2^* were chosen to be 1.1 times their respective output powers in the reference design, and $C = 1000$ is the penalty factor. Note that in the reference design, some of the rods in the fourth and sixth rows are off the square grid. However, the starting point of our optimization process has these rods on the grid to allow greater flexibility in choice of radii. The entire optimization process took 1.5 hours on a 3.4GHz Intel Core i7-6700 CPU, where each rod was expanded into 21 cylindrical waves and the solver tolerance was 10^{-6} .

Figures 2(a) and 2(b) show the electric field amplitude in the reference design when excited by a $1 \mu\text{A}$ current filament with wavelengths λ_1 and λ_2 , while Figs. 2(c) and 2(d) show the optimized device. The left waveguide in the optimized design exhibits stronger localization for λ_1 and less crosstalk from λ_2 . The radii in the optimized device are less regular, with both symmetric and asymmetric deformations surrounding both exit waveguides, for example, on the second column from the left. We also see a gradual tapering of the radii around the input.

In Fig. 3 we depict in detail the power density entering through the top of the device and exiting the desired side for each frequency. Visibly more power is launched through the centers of the desired outputs (Figs. 3(b,d)), at the expense of slightly larger side lobes. The power entering

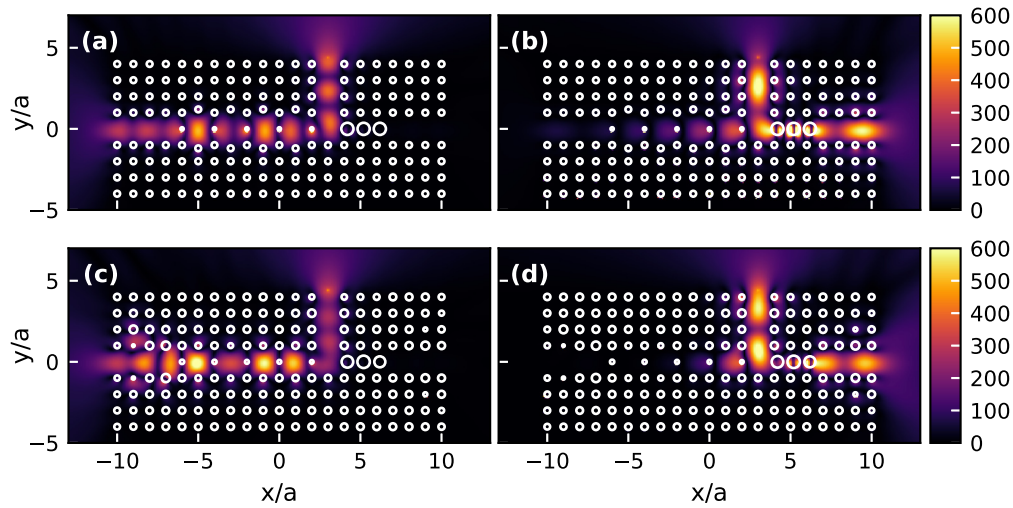


Fig. 2. Amplitude of the electric field E_z in the diplexer when excited by a current filament. (a) Reference design with λ_1 , (b) reference design with λ_2 , (c) optimized design with λ_1 , (d) optimized design with λ_2 .

and exiting the devices is computed as follows: the power density is integrated along the entire top border as well as along each side border. The calculation was performed in this manner to account for all of the power flowing through the device, including through the bulk photonic crystal. For presentation purposes we omitted those parts of Figs. 3(a,c) where the power density is essentially zero despite being integrated over. The optimized device has better matching to the source, with total power flow through the top border of $55.48 \mu\text{W m}^{-1}$ vs. $54.39 \mu\text{W m}^{-1}$ in the reference design for λ_1 , and $102.07 \mu\text{W m}^{-1}$ vs. $68.55 \mu\text{W m}^{-1}$ for λ_2 . This is unsurprising since the reference design was originally simulated with a different source type; however, based on these results we expect the optimization to also match well to other source types.

The ratios between the power exiting the sides and bottom, to the power entering the top of the devices are summarized in Table 1, where the power is calculated according to Eq. (1) using the complete side length. Here we see that for the optimized device, the percentage of the power exiting the desired side is increased for λ_2 and unchanged for λ_1 , and that the power at the undesired side is reduced for both frequencies. Accordingly, the crosstalk for λ_1 is -24.5 dB before optimization and -27.4 dB after, while for λ_2 optimization reduced the crosstalk from -19.3 dB to -44.0 dB. The crosstalk was calculated by dividing the unwanted power transmission ratio by that of the desired wavelength, in order to account for the different total power entering each device for each frequency, as exemplified in Fig. 3. We observe that due to our optimization of several objectives simultaneously, power loss through the bottom of the optimized device slightly increased for λ_1 .

Table 1. Power Transmission for Diplexer

	λ_1 , left	λ_1 , right	λ_1 , bottom	λ_2 , left	λ_2 , right	λ_2 , bottom
Reference	99.5%	0.35%	0.12%	1.17%	98.6%	0.24%
Optimized	99.5%	0.18%	0.33%	0.004%	99.8%	0.19%

In Fig. 4, we present the power transmission of both reference and optimized designs for a range of different wavelengths. The total power flow in the left and right directions is shown in Fig. 4(a), where we observe once again that the power transmitted for λ_2 (left vertical line) is much higher

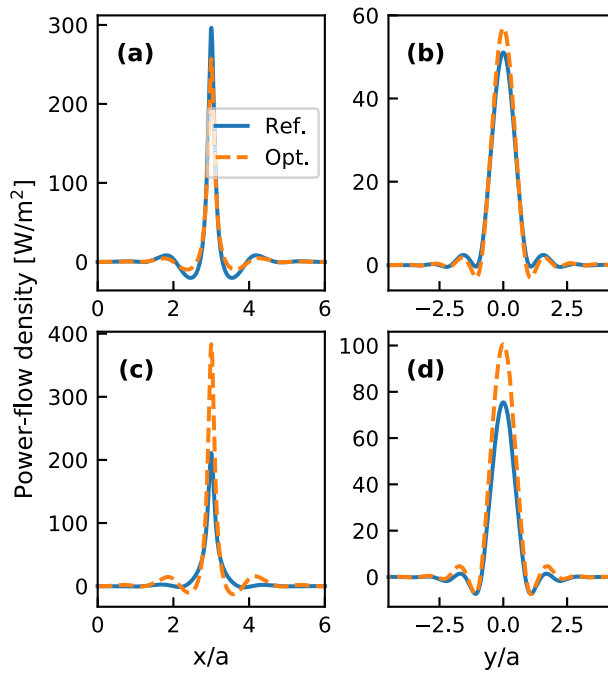


Fig. 3. Power density entering the top and exiting the desired sides of the reference and optimized diplexers. (a) λ_1 power entering the top, (b) λ_1 exiting the left, (c) λ_2 entering the top, (d) λ_2 exiting the right.

in the optimized design. For $a/\lambda = 0.35 - 0.38$, power flow to both sides drops precipitously in the optimized device, but only on the right-hand side for the reference. Figure 4(b) shows the same power normalized by the power entering the device for each wavelength. Interestingly, there is a wider range of frequencies surrounding λ_2 where both the power and the normalized transmission to the left are large for the optimized device than for the reference design, despite the optimization being performed at only two wavelengths.

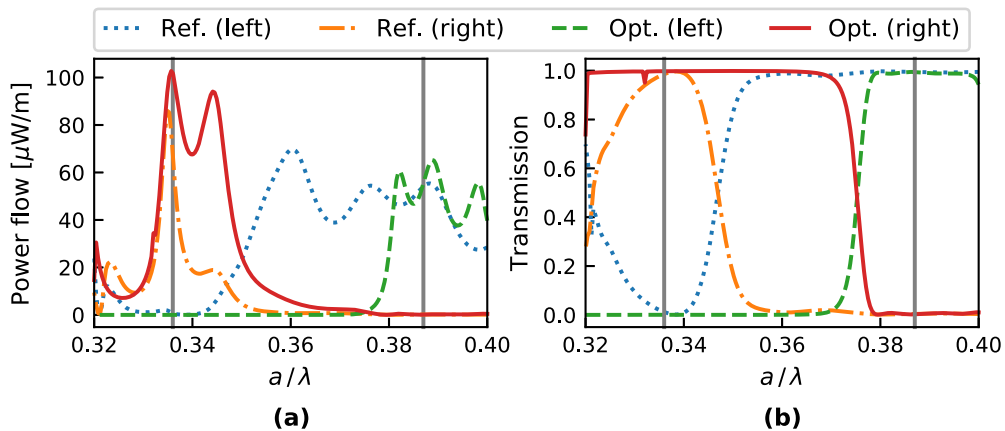


Fig. 4. Power flow to the left and right sides of the reference and optimized diplexers. (a) Absolute. (b) Normalized by power entering the device. Vertical lines indicate the frequencies of interest λ_1, λ_2 .

Figure 5 shows the second device we designed, an optical diode structure that permits light propagation in one direction while restricting it in the opposite direction. This device was achieved by optimizing the radii of 70 dielectric rods ordered in a triangular lattice for maximizing left-to-right power propagation from a plane wave while minimizing right-to-left propagation. In this case, the optimization required 20 minutes before convergence. Each rod was expanded into 21 cylindrical waves and a relative tolerance of 10^{-6} for the electromagnetic solver.

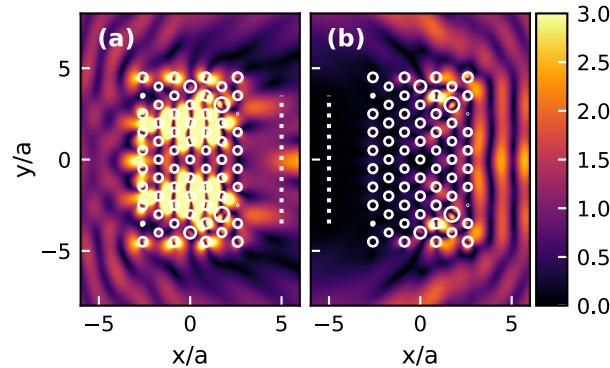


Fig. 5. Amplitude of E_z for the designed optical diode in response to a unit plane wave. (a) Left-to-right propagation. (b) Right-to-left propagation. Dotted line indicates where power flow was optimized and calculated.

The optimization starting point had $r/a = 0.2$ for all rods, where the cell size is $a = 600$ nm and the desired operating wavelength is $\lambda = 1500$ nm, both of which correspond to a normalized frequency of $\omega a/2\pi c = 0.4$, and we used a wavelength-dependent refractive index for the silicon ($n = 3.48$ at $\lambda = 1500$ nm) [30].

The objective in this case was maximizing the power P_r propagating through the right side for plane waves originating from the left, while minimizing the power P_l on the left side from plane waves propagating in the $x = -\infty$ direction. P_r, P_l were computed by integrating the \hat{x} -directed power flow density along the dotted lines in Fig. 5. This objective is expressed by minimizing the function

$$f = \frac{1}{P_r} \left(1 + C \frac{|P_l|}{P_r} \right), \quad (6)$$

where $C = 1000$ was chosen as the transmission ratio penalty factor.

Setting the optimization starting point of $r/a = 0.2$ for all rods places λ in a complete photonic bandgap, as depicted in Fig. 6, which shows the band structure for the infinitely periodic version of the device. This initial structure does not allow propagation of $\pm\hat{x}$ -directed plane waves, despite having only 7 cells in the x direction. The choice of the initial device was such that the bandgap would prevent propagation in both directions, and the optimization process would tweak the device to permit one-directional propagation. Indeed, we can see in Fig. 5(a) that the electric field originating from the left propagates through the device, and is magnified in certain regions on the right. On the other hand, when the field originates from the right as in Fig. 5(b), the device creates a shaded area on the left with near-zero electric field amplitude. Due to the optimization, all of the radii changed by at least 2.5%, with the most radical changes at the corners of the structure, where a few rods have been nearly eliminated from the structure and others have doubled in size.

We also investigated the performance of this device for a range of wavelengths surrounding λ , namely 1400 to 1600 nm. In Fig. 7(a), we have the power flow measured in both directions, normalized by the power flow in the absence of the device, P_0 . At 1500 nm, we have $P_r = 1.37P_0$ and $P_l = 2.06 \times 10^{-6}P_0$, as well as a FWHM of 9.65 nm for P_r . We may have P_r/P_0 greater

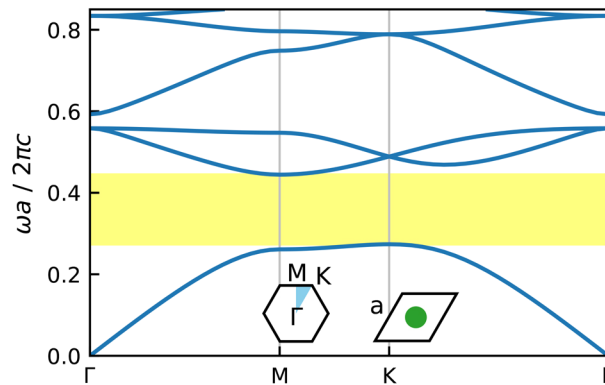


Fig. 6. Photonic band structure for a triangular array of dielectric ($n = 3.48$) rods of radius $r/a = 0.2$ in air, for TM polarization. The insets depict the irreducible Brillouin zone in light blue as well as the unit cell.

than unity, partially because the height of the device exceeds the length of the line on which the power is measured. The ratio between right- and left-propagating power is depicted with a solid line in Fig. 7(b), where a transmission ratio of 58.2 dB is achieved. The stark narrowbandedness exhibited in both plots is expected since the optimization was performed for a single frequency.

Lastly, we optimized the same initial triangular lattice for one-way transmission in the presence of current filament excitation, placed at $(\pm 5a, 0)$. The minimization process in this case required 19 minutes. This device had a transmission ratio of 46 dB at $\lambda = 1500$ nm, as plotted with a dashed line in Fig. 7(b). The resulting structure, shown in Fig. 8, is irregular as well, with a large variance of the radii present in the structure. In this case, the power density distribution after optimization is concentrated in two lobes, as opposed to the strong central lobe in the plane-wave case. Similarly to the optimized diplexer, there is tapering of the radii in the vicinity of the source on the left. The high transmission ratios for both types of excitation suggest that our method may find optimal devices for different incident fields.

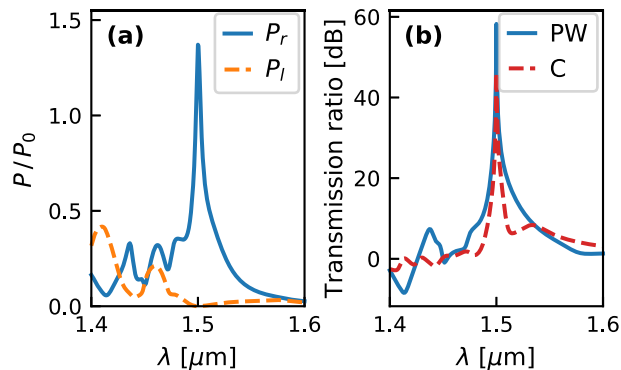


Fig. 7. (a) Power transmission spectrum in both directions, normalized by the power flow without the device. (b) Transmission ratio between right- and left-propagating light for the device that was optimized for excitation by plane wave (solid line) and current filament (dashed).

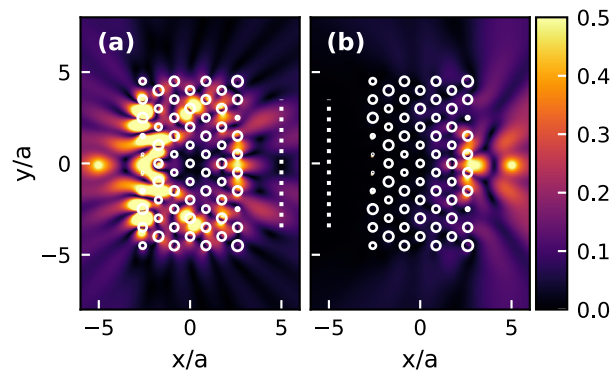


Fig. 8. Amplitude of E_z for the designed optical diode in response to a 1 nA current filament. (a) Left-to-right propagation. (b) Right-to-left propagation. Dotted line indicates where power flow was optimized and calculated.

4. Conclusion

In summary, we designed two aperiodic devices, each consisting of a collection of dielectric rods, using optimization. The first device, a diplexer, was the result of optimizing an existing design and yielded better performance in our simulations. Next, we designed an optical diode to realize passive one-way transmission. Here we began with a uniform structure based on the photonic bandgap and obtained a device with a high transmission ratio. In both cases, the resulting optimized devices had rather irregular and unintuitive radius distributions, which agrees with the suggestion that irregular structures introduce additional degrees of freedom which may be exploited for precise electromagnetic field control. These devices can find potential use in optical computing, and the method we employed in this work shows promise for designing other dielectric photonic devices.

Funding

Austrian Science Fund (FWF) (START Project Y 660).

References

1. H. J. Caulfield and S. Dolev, "Why future supercomputing requires optics," *Nat. Photonics* **4**(5), 261–263 (2010).
2. Y. Liu, F. Qin, Z.-M. Meng, F. Zhou, Q.-H. Mao, and Z.-Y. Li, "All-optical logic gates based on two-dimensional low-refractive-index nonlinear photonic crystal slabs," *Opt. Express* **19**(3), 1945–1953 (2011).
3. V. Jandieri, R. Khomeriki, and D. Erni, "Realization of true all-optical AND logic gate based on nonlinear coupled air-hole type photonic crystal waveguides," *Opt. Express* **26**(16), 19845–19853 (2018).
4. H. Takahashi, S. Suzuki, K. Kato, and I. Nishi, "Arrayed-waveguide grating for wavelength division multi/demultiplexer with nanometre resolution," *Electron. Lett.* **26**(2), 87–88 (1990).
5. Y. Tan, H. Wu, S. Wang, C. Li, and D. Dai, "Silicon-based hybrid demultiplexer for wavelength- and mode-division multiplexing," *Opt. Lett.* **43**(9), 1962–1965 (2018).
6. A. Y. Piggott, J. Lu, K. G. Lagoudakis, J. Petykiewicz, T. M. Babinec, and J. Vučković, "Inverse design and demonstration of a compact and broadband on-chip wavelength demultiplexer," *Nat. Photonics* **9**(6), 374–377 (2015).
7. E. Centeno, B. Guizal, and D. Felbacq, "Multiplexing and demultiplexing with photonic crystals," *J. Opt. A: Pure Appl. Opt.* **1**(5), L10–L13 (1999).
8. A. Sharkawy, S. Shi, and D. W. Prather, "Multichannel wavelength division multiplexing with photonic crystals," *Appl. Opt.* **40**(14), 2247–2252 (2001).
9. V. Liu, Y. Jiao, D. A. B. Miller, and S. Fan, "Design methodology for compact photonic-crystal-based wavelength division multiplexers," *Opt. Lett.* **36**(4), 591–593 (2011).
10. R. Philip, M. Anija, C. S. Yelleswarapu, and D. V. G. L. N. Rao, "Passive all-optical diode using asymmetric nonlinear absorption," *Appl. Phys. Lett.* **91**(14), 141118 (2007).

11. M. Vanwolleghem, X. Checoury, W. Śmigaj, B. Gralak, L. Magdenko, K. Postava, B. Dagens, P. Beauvillain, and J.-M. Lourtioz, "Unidirectional band gaps in uniformly magnetized two-dimensional magnetophotonic crystals," *Phys. Rev. B* **80**(12), 121102 (2009).
12. C. Menzel, C. Helgert, C. Rockstuhl, E.-B. Kley, A. Tünnermann, T. Pertsch, and F. Lederer, "Asymmetric transmission of linearly polarized light at optical metamaterials," *Phys. Rev. Lett.* **104**(25), 253902 (2010).
13. Y. Xu, C. Gu, B. Hou, Y. Lai, J. Li, and H. Chen, "Broadband asymmetric waveguiding of light without polarization limitations," *Nat. Commun.* **4**(1), 2561 (2013).
14. M. Stolarek, D. Yavorskiy, R. Kotyński, C. J. Z. Rodríguez, J. Łusakowski, and T. Szoplik, "Asymmetric transmission of terahertz radiation through a double grating," *Opt. Lett.* **38**(6), 839–841 (2013).
15. P. Xu, X. Lv, J. Chen, Y. Li, J. Qian, Z. Chen, J. Qi, Q. Sun, and J. Xu, "Dichroic optical diode transmission in two dislocated parallel metallic gratings," *Nanoscale Res. Lett.* **13**(1), 392 (2018).
16. Y. Zhang, Q. Kan, and G. P. Wang, "One-way optical transmission in silicon grating-photonic crystal structures," *Opt. Lett.* **39**(16), 4934–4937 (2014).
17. D. Liu, S. Hu, and Y. Gao, "One-way optical transmission in silicon photonic crystal heterojunction with circular and square scatterers," *Phys. Lett. A* **381**(25-26), 2131–2135 (2017).
18. E. Bor, M. Turduev, U. G. Yasa, H. Kurt, and K. Staliunas, "Asymmetric light transmission effect based on an evolutionary optimized semi-dirac cone dispersion photonic structure," *Phys. Rev. B* **98**(24), 245112 (2018).
19. Y.-C. Hsueh and K. J. Webb, "Electromagnetic field control with binary aperiodic nanostructures," *J. Opt. Soc. Am. B* **34**(10), 2059–2071 (2017).
20. B. Blankrot and C. Heitzinger, "Efficient computational design and optimization of dielectric metamaterial devices," <http://arxiv.org/abs/1804.09489> (2018). *Submitted for publication.*
21. B. Blankrot and C. Heitzinger, "Automated design of photonic crystal demultiplexers," in *2018 12th International Congress on Artificial Materials for Novel Wave Phenomena (Metamaterials)*, (Espoo, Finland, 2018), pp. 55, 57.
22. N. A. Gumerov and R. Duraiswami, "A scalar potential formulation and translation theory for the time-harmonic maxwell equations," *J. Comput. Phys.* **225**(1), 206–236 (2007).
23. J. Lai, M. Kobayashi, and L. Greengard, "A fast solver for multi-particle scattering in a layered medium," *Opt. Express* **22**(17), 20481–20499 (2014).
24. J. S. Jensen and O. Sigmund, "Systematic design of photonic crystal structures using topology optimization: Low-loss waveguide bends," *Appl. Phys. Lett.* **84**(12), 2022–2024 (2004).
25. M. Minkov and V. Savona, "Automated optimization of photonic crystal slab cavities," *Sci. Rep.* **4**(1), 5124 (2014).
26. C. Valagiannopoulos and P. G. Lagoudakis, "Photonic crystals for optimal color conversion in light-emitting diodes: a semi-analytical approach," *J. Opt. Soc. Am. B* **35**(5), 1105–1112 (2018).
27. P. Seliger, M. Mahvash, C. Wang, and A. F. J. Levi, "Optimization of aperiodic dielectric structures," *J. Appl. Phys.* **100**(3), 034310 (2006).
28. R. Coifman, V. Rokhlin, and S. Wandzura, "The fast multipole method for the wave equation: a pedestrian prescription," *IEEE Antennas Propag. Mag.* **35**(3), 7–12 (1993).
29. J. Smajic, C. Hafner, and D. Erni, "On the design of photonic crystal multiplexers," *Opt. Express* **11**(6), 566–571 (2003).
30. H. H. Li, "Refractive index of silicon and germanium and its wavelength and temperature derivatives," *J. Phys. Chem. Ref. Data* **9**(3), 561–658 (1980).